I

Subwavelength resolution

1 Subwavelength imaging by arrays of metallic rods *Pavel A. Belov, Mário G. Silveirinha, Constantin R. Simovski, and Yang Hao* **1**-1
Introduction • Wire medium lens • Transmission and reflection characteristics of wire medium slabs • Magnifying and demagnifying lenses with super-resolution • Imaging at terahertz frequencies and beyond

1

Subwavelength imaging by arrays of metallic rods

Pavel A. Belov
Queen Mary University of London, UK

Mário G. Silveirinha
University of Coimbra, Portugal

Constantin R. Simovski
Helsinki University of Technology, Finland

Yang Hao
Queen Mary University of London, UK

1.1 Introduction 1-1
1.2 Wire medium lens 1-4
1.3 Transmission and reflection characteristics of wire medium slabs 1-8
Analytical modeling • Parametric study of reflection and transmission properties
1.4 Magnifying and demagnifying lenses with super-resolution 1-12
1.5 Imaging at terahertz frequencies and beyond 1-14
References 1-18

1.1 Introduction

Lens-based imaging devices such as conventional microscopes cannot provide resolution better than $\lambda/2$, where λ is the wavelength of radiation. This restriction is known as the diffraction limit, and holds irrespectively of the frequency of operation - from microwave frequencies up to the visible range. Conventional lenses operate only with the far-field of the source, which is formed by propagating spatial harmonics. The information related to the near-field of the source is transported by evanescent spatial harmonics, which exhibit exponential decay in all natural materials as well as in free space. For this reason, the subwavelength details of the near-field are not directly accessible with conventional imaging systems. In practice, the near-field can be scanned, point by point, using small near-field probes. However, scanning near-field microscopy is a rather slow process, and thus lenses that may enable the simultaneous imaging of the whole region of interest with super-resolution would be extremely useful.

The diffraction limit can be surpassed only if one adopts a conceptually different imaging technique. In order to obtain imaging with subwavelength resolution, it may be necessary to overstep beyond the frontiers of naturally available materials and to use specially engineered artificial media with electromagnetic properties not readily available in nature. In recent years, several techniques have been put forward aiming at imaging with super-resolution in different ranges of the electromagnetic spectrum. These proposals include perfect lenses [1], silver superlenses [2], hyperlenses [3, 4, 5, 6, 7], and stimulated emission depletion (STED) fluorescence microscopes [8]. Another option, which is the topic of the present Chapter, is based on the use of materials with extreme optical anisotropy.

0-8493-8597-0/01/$0.00+$1.50

Let us consider an uniaxial dielectric medium with permittivity dyadic of the form:

$$\underline{\boldsymbol{\varepsilon}} = \begin{pmatrix} \varepsilon_{xx} & 0 & 0 \\ 0 & \varepsilon & 0 \\ 0 & 0 & \varepsilon \end{pmatrix}. \tag{1.1}$$

The dispersion equation for extraordinary waves in such medium reads:

$$\frac{k_x^2}{\varepsilon} + \frac{k_y^2 + k_z^2}{\varepsilon_{xx}} = \frac{\omega^2}{c^2}, \tag{1.2}$$

where k_x, k_y, k_z are the components of wave vector $\mathbf{k}$, ω is the frequency of operation and c is the speed of light in vacuum.

If the material is characterized by extreme optical anisotropy such that $|\epsilon_{xx}| \gg \epsilon$, then (1.2) has the following solution:

$$k_x = \pm\sqrt{\varepsilon}\frac{\omega}{c} \text{ and } k_y, k_z \text{ are arbitrary.} \tag{1.3}$$

Therefore, all extraordinary waves in a medium with extreme optical anisotropy are dispersionless: the electromagnetic waves travel along the optical axis of the material with a fixed phase velocity independently of the transverse phase variations. Note that ϵ_{xx} does not to have to be necessarily a real number. It may be a complex number with a large absolute value. The imaginary part of ϵ_{xx} representing losses has very little influence on the wave propagation.

To a good approximation, the class of dielectrics with extreme optical anisotropy can be described by a dielectric function of the form

$$\underline{\boldsymbol{\varepsilon}} = \begin{pmatrix} \infty & 0 & 0 \\ 0 & \varepsilon & 0 \\ 0 & 0 & \varepsilon \end{pmatrix}. \tag{1.4}$$

The infinite value appearing in (1.4) should not be treated as something exceptional or unusual. The corresponding material relations read as $E_x = 0$, $D_y = \varepsilon E_y$ and $D_z = \varepsilon E_z$. This actually means that the medium is perfectly conducting along x-direction.

The latter fact gives a hint how media with extreme optical anisotropy can be created artificially. An array of parallel metallic wires, also known as "wire medium" [9], may provide the necessary properties at frequencies up to the infrared band [10]. In the visible range, one of the options may be a layered-metal dielectric structure [11] which has an effective permittivity consistent with (1.4).

Materials with extreme anisotropy have remarkable properties: all the extraordinary waves supported by the media are propagating waves (see Fig.1.1). Thus, theoretically, it is possible to transport an arbitrary field distribution with suitable polarization through such material with no loss of resolution. Lenses formed by slabs of such materials provide a unique opportunity to transmit the near-field with super-resolution. At the front interface with free-space, the evanescent waves are transformed into propagating waves, which prevents their decay and preserves the subwavelength information. The propagating waves travel through the slab and reproduce the image at the back interface of the lens. This phenomenon is known as *canalization* [12]. This regime is especially appropriate for the transmission of images with super-resolution over significant distances in terms of the wavelength. This effect cannot be achieved using other available imaging techniques.

Basically, the canalization regime is very similar to the fiber-optic effect which is observed in the "TV rock" (see Fig. 1.2). This mineral consists of parallel tiny optical fibers which

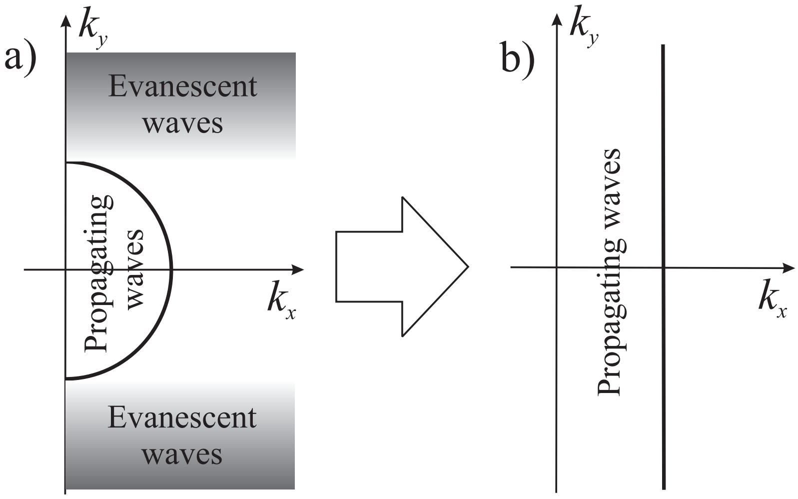

FIGURE 1.1 (a) Isofrequency contours in a isotropic material (e.g. free-space). For $|k_y| > \omega/c$ the spatial harmonics correspond to evanescent waves (shaded region). (b) Isofrequency contours in a material with extreme optical anisotropy. All the spatial harmonics are propagating waves.

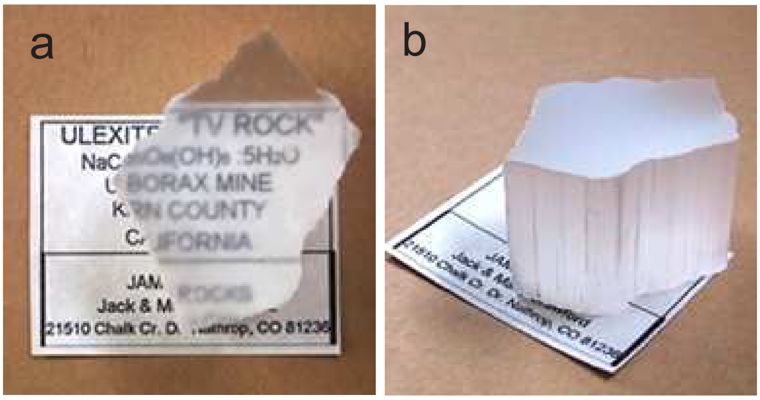

FIGURE 1.2 The fiber-optic effect by "TV rock", a mineral Ulexite ($NaCaB_5O_9{\cdot}8H_2O$, hydrated sodium calcium borate hydroxide). a) Top view. b) Side view.

are capable of transporting images pixel by pixel. The significant difference is that the canalization regime provides super-resolution, whereas the resolution provided by the TV rock is determined by dimensions of the fibers which are greater than the wavelength. In order to get super-resolution one has to use an array of subwavelength waveguides such as an array of metallic wires.

An alternative and widely known opportunity of subwavelength imaging is the perfect lens concept [1]. It is based on the amplification of evanescent harmonics by a metamaterial, rather than on their conversion into propagating waves. This may enable imaging objects which are placed at some significant distance from the lens interface, like buried objects. However, the perfect lens relies on the resonant excitation of surface plasmon-polaritons at the interfaces of a metamaterial slab, and hence it is very sensitive to losses [13]. The amplification of the evanescent waves requires such a low level of losses in the metamaterial that it may be extremely difficult to achieve in practice. Even if the current race to create the metamaterial required for the implementation of the perfect lens in the optical range [14, 15, 16, 17] is successfully accomplished then such material will be inevitably lossy and its use as a subwavelength imaging device may be of limited interest.

The effect of losses on the canalization regime is much less restrictive. Losses cause the decay of propagating waves inside of the material, but the decaying factor is the same for the whole spatial spectrum. This means that losses cause only a degradation of intensity but do not corrupt the form of the image [18]. This makes lenses operating in the canalization regime easier to fabricate as compared to perfect lenses, regardless of the frequency range of operation.

1.2 Wire medium lens

In principle, materials with extreme optical anisotropy are not directly available in nature. However, these materials may be synthesized as microstructured materials. In particular, an array of long thin parallel metallic wires (Fig. 1.3) is characterized by extreme anisotropy in the long wavelength limit. The emergence of extreme anisotropy in this structure is due to the strong electric polarizability of the rods along the direction of the axes. The wire medium supports electromagnetic modes that are effectively described by a dielectric function of the form (1.4) with ε equal to the permittivity of the host matrix [9] *. Such "transmission line" modes travel along the wires with the speed of light in the host medium, and can have an arbitrary transverse wave vector.

A planar wire medium slab (Fig. 1.3) enables the transformation of the near-field produced by a source placed in the vicinity of the slab into propagating transmission line modes. These modes propagate along the direction normal to the interfaces and transfer the distribution of electric field from the front interface of the lens to the back interface without distortion, closely mimicking the behavior of a material with extreme anisotropy.

In a different but equivalent perspective, the slab of a wire medium may also be regarded as a bundle of very subwavelength waveguides performing pixel to pixel imaging. Each wire plays the role of a waveguide delivering information from one side of the lens to the other. The electric field distribution transported by a specific wire is approximately radial, and due to this reason the waveguides are nearly decoupled. This enables the propagation of waves along neighboring wires with a negligibly small interaction. The imaging resolution is approximately two periods of the wire medium [19], and, in principle, can be made as small as required by a given application.

In contrast to conventional lenses, near-field lenses have to be placed in the close vicinity of the source in order to capture evanescent waves. Thus, it is important to ensure that the lens does not distort the source field distribution. An ideal near-field lens should not produce any reflections. The problem of possible harmful reflections from a slab of a material with extreme anisotropy can be eliminated by properly choosing its thickness so that it operates as a Fabry-Perot resonator. The thickness should be equal to an integer number of half-wavelengths inside of the host material. In the case of an ideal material described by the

*It is important to mention that the description of the wire medium using the permittivity model (1.4) is only a rough approximation. In reality, the wire medium is a spatially dispersive material and thus its electrodynamics is more complicated than suggested by (1.4) [9]. However, for very long wavelengths the spatial dispersion effects are to some extent of second order [19], and the dielectric function (1.4) may describe fairly well the response of the material. These ideas are discussed with more details in Sect. 1.3.

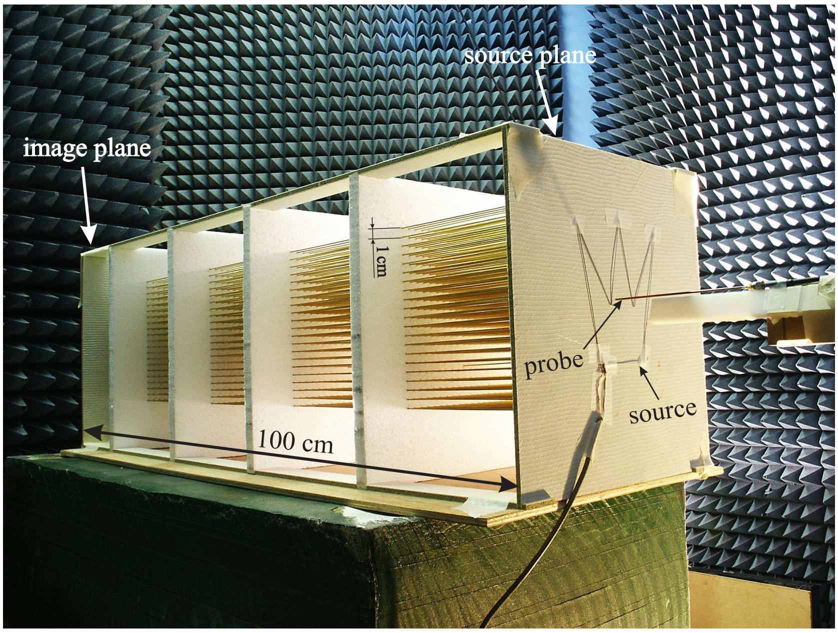

FIGURE 1.3 Photograph of the wire medium lens used in experiment [20]: 21 x 21 array of parallel 1-meter long aluminium wires. The period of the array is 1 cm. The radius of the wires is 1 mm. The source in the form of a crown is adjacent to the front interface of the lens. The source is fed by a coaxial cable connected to a network analyzer. The small electric probe used for near field scan is shown together with the supporting arm.

dielectric function (1.4), the Fabry-Perot condition is verified simultaneously for all angles of incidence, including evanescent waves. This collective resonance makes the lens virtually transparent to any propagating or evanescent wave. This outstanding property is justified by the fact that all transmission line modes travel across the slab with the same phase velocity, irrespectively of transverse wave vector. Thus, the total electrical length of the slab remains the same for all possible incidence angles.

A prototype of a 1-meter long wire medium lens with 1 cm period is reported in Fig. 1.3. The photograph shows the lens located in the anechoic chamber together with the setup for near-field scan. The lens was designed to operate at frequencies around 150n MHz, which correspond to Fabry-Perot resonances of the n-th order [20]. The measurements were made at frequencies around 900 and 1050 MHz corresponding to Fabry-Perot resonances of the 6-th and 7-th orders, respectively. This prototype is about 7 times longer than the 15-cm long lens used for the preliminary experiments reported in [21, 22].

A wire antenna shaped as a crown was taken as the near-field source. The source was placed near the front interface of the wire medium lens as shown in Fig. 1.3, and the near-field was scanned using an automatic mechanical planar near-field scanner at a distance of 2 mm from the front and back interfaces of the lens (source and image planes). In order to confirm that the lens does not perturb or distort the near-field of the source, the collected data were compared with the reference near-field distributions obtained by scanning the near field created by the source in free space. The results of the near-field scan at 898 and 1038 MHz are reported in Figs. 1.4 and 1.5. A near-field distribution reproducing the crown shape is clearly visible at the image plane. It is practically indistinguishable from the distributions in the source plane both with and without presence of the wire medium lens.

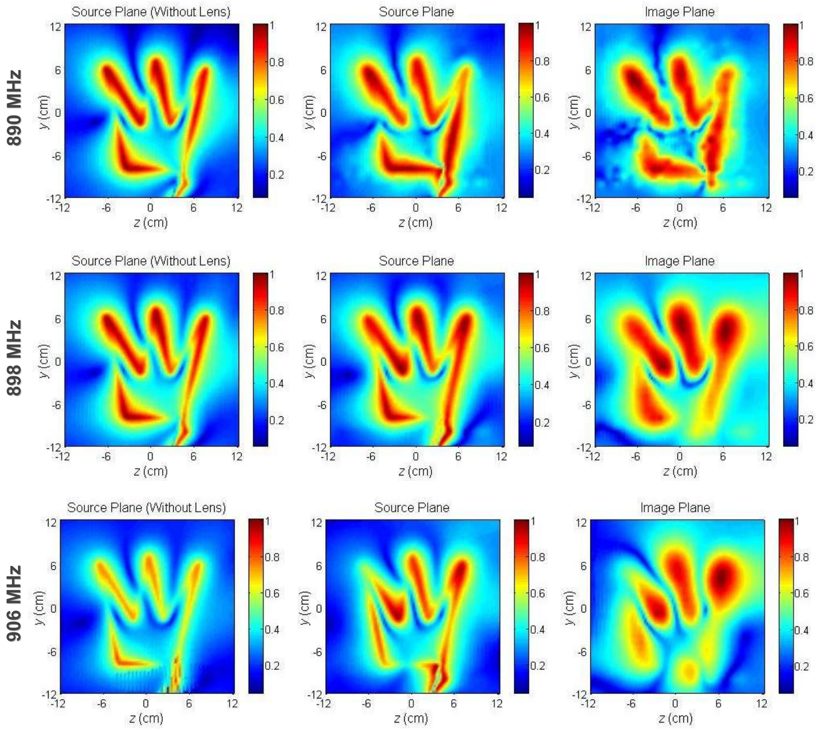

FIGURE 1.4 Results of the near-field scan at the source plane (2 mm away from the front interface of the lens) without (left column) and with (central column) the wire medium lens and (right column) at the image plane (2 mm away from the back interface of the lens) at 890, 898 and 906 MHz .

Despite the distance in between the source and image planes at 898 and 1038 MHz being as large as 3 and 3.5 wavelengths, respectively, the imaging resolution is about two periods of the wire medium (2 cm), which in terms of the wavelength corresponds to $\lambda/15$. To the best of our knowledge, this is up to date the only demonstration of subwavelength imaging with such fine resolution over a distance much larger than the wavelength. In all other subwavelength imaging experiments reported in the literature, the distance between the source and image planes was only a small fraction of the wavelength, whereas the imaging resolution was much worse.

The near field scan results reported in Figs. 1.4 and 1.5 enable to clarify how the resolution of the wire medium lens depends on the frequency of operation. As mentioned before, the lens thickness is supposed to verify the Fabry-Perot condition. Actually, as it was shown in [19], the best imaging is achieved at a frequency slightly below the Fabry-Perot condition. At higher frequencies subwavelength imaging is still observed, but with worse resolution. This can be clearly seen in Fig. 1.4: the widths of the lines at the image plane become wider above the Fabry-Perot resonance. The amount of reflection provided by the wire medium slab at these frequencies is quite small: in Fig. 1.4 the difference between the source plane distributions with and without presence of the lens is not significant. These properties are typical of wire medium lenses [19, 22]. At frequencies below the Fabry-Perot resonance the imaging is disturbed by the excitation of surface waves at both the front and back interfaces of the lens. This effect can be clearly seen in Fig. 1.5 where the image and the source plane field distributions in the presence of the lens at frequencies below Fabry-Perot resonance are

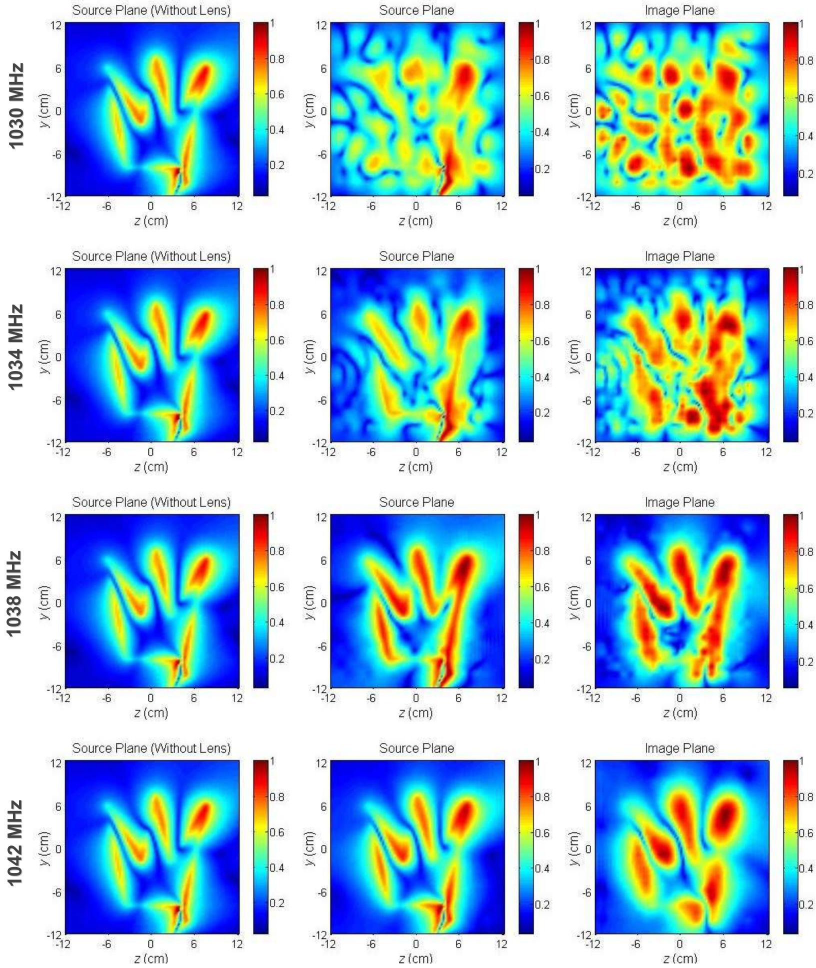

FIGURE 1.5 Results of the near-field scan at the source plane (2 mm away from the front interface of the lens) without (left column) and with (central column) the wire medium lens and (right column) at the image plane (2 mm away from the back interface of the lens) at 1034, 1038, 1042 and 1046 MHz .

completely distorted by the ripples caused by the excitation of surface wave modes [19, 22]. These properties will be further discussed in Sect. 1.3.

Despite the described dependency of the resolution on frequency, the resolving capabilities of wire medium lenses are reasonably wide-band. The actual bandwidth of operation depends on the complexity of the near-field source and on its sensitivity to external fields [22], but it cannot be smaller than the fundamental theoretical limit formulated in [19]. In practice, a bandwidth of the order of a few percents is observed: 4.5% in [22] for a half-wavelength thick lens with a complex meander-like source, and 2% in experiment with a 3 wavelength thick lens with a crown-shaped source [20]. For less complex sources the same lenses may provide much better bandwidth. For example, in [21] the bandwidth was 18%, for a half-wavelength thick lens with a source shaped in the form of a “P” letter.

In principle, the resolution of the wire medium lens can be made as fine as required by a specific application by just using materials with smaller periods. For example, instead of a lens with 1 cm period and wires with 1 mm radius (as in Fig. 1.3) providing resolution $\lambda/15$, one can manufacture structure with 1 mm period and 100μm radius of wires which would provide a resolution of $\lambda/150$, and so on *. Basically, the minimum achievable resolution is limited only be the manufacturing capabilities and by the skin depth of the metal. In order to operate the wire medium in the canalization regime it is necessary that the radius of the rods is greater than the skin depth of the metal [23]. At microwaves, the skin depth of good metals is of the order of a few μm, and is thus negligible. The ultimate limit of resolution of wire medium lenses in different frequency regimes is discussed in section 1.5.

1.3 Transmission and reflection characteristics of wire medium slabs

The imaging properties of wire medium lenses can be predicted to a very good approximation using homogenization methods. In this section, we briefly review such theory, and discuss with some detail the transmission and reflection characteristics of wire medium lenses.

1.3.1 Analytical modeling

As mentioned in Sect. 1.2, an array of metallic wires behaves to a first approximation as a material with extreme optical anisotropy characterized by the dielectric function (1.4). This description is particularly accurate when the wires are very densely packed, so that the ratio a/d is very small (a is the lattice period, and d is the length of the wires).

A more accurate homogenization model for the wire medium was derived in Ref. [9], where it was demonstrated that the material is characterized by strong spatial dispersion even at low frequencies. Supposing that the host material is air, it was shown that the wire medium can be described by the dielectric function (1.1), with $\varepsilon = 1$ and

$$\varepsilon_{xx}(\omega, q_x) = 1 - \frac{k_p^2}{k^2 - q_x^2}. \tag{1.5}$$

In the above, q_x is the x-component of wave vector $\mathbf{q}$, $k = \omega/c$ is the wave number of the host medium, c is the speed of light, and $k_p = \omega_p/c$ is the wave number corresponding to the plasma frequency ω_p. The plasma frequency depends on the lattice period a and on the radius of wires r [24]. For an array of metallic wires arranged in a square lattice, we have that:

$$k_p^2 = \frac{2\pi/a^2}{\ln \frac{a}{2\pi r} + 0.5275}. \tag{1.6}$$

Let us consider a slab of wire medium with thickness d and suppose that the wires stand in free-space and are normal to the interface. Suppose that a plane wave with TM polarization (magnetic field is parallel to the interface) illuminates the wire medium slab. We denote the transverse component of the wave vector of the incoming wave by k_y, and the corresponding propagation constant along x by $\gamma_x = \sqrt{k_y^2 - k^2}$. The value of γ_x is purely imaginary if $|k_y| < k$ (propagating modes in free space), but it becomes a real number if $|k_y| > k$ (evanescent modes in free space, i.e. the sub-wavelength spatial spectrum).

*However, one should keep in mind that to take advantage of a lens with a better resolution the source may need to be placed closer to the front interface.

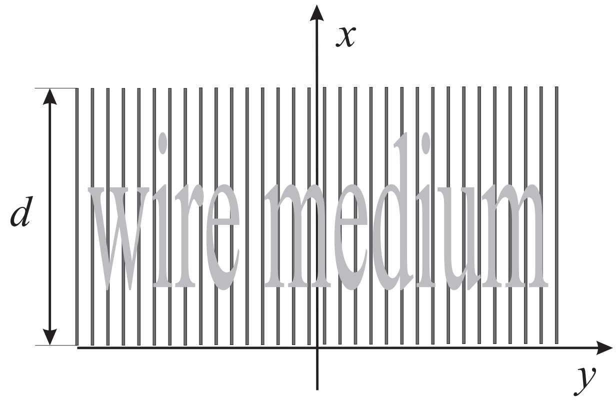

FIGURE 1.6 The wire medium slab. The structure is unbounded along the y- and z-directions.

The incident plane wave excites two types of waves in the wire medium: the extraordinary wave (TM mode) and the transmission line (TEM) mode [9]. This latter mode behaves exactly as if it were propagating in a material with extreme optical anisotropy with dielectric function given by (1.4). The effect of spatial dispersion is to excite the “additional” extraordinary (TM) wave.

The following analytical expressions for transmission and reflection coefficients for the slab were derived in [19] using the additional boundary condition formulated in [25]:

$$\begin{aligned} R = 1 &- \frac{1}{1 + \frac{\gamma_{\mathrm{TM}} k_y^2}{\gamma_x (k_y^2 + k_p^2)} \tanh(\frac{\gamma_{\mathrm{TM}} d}{2}) - \frac{k k_p^2}{\gamma_x (k_y^2 + k_p^2)} \tan(\frac{kd}{2})} \\ &- \frac{1}{1 + \frac{\gamma_{\mathrm{TM}} k_y^2}{\gamma_x (k_y^2 + k_p^2)} \mathrm{ctanh}(\frac{\gamma_{\mathrm{TM}} d}{2}) + \frac{k k_p^2}{\gamma_x (k_y^2 + k_p^2)} \mathrm{ctan}(\frac{kd}{2})}, \end{aligned} \tag{1.7}$$

$$\begin{aligned} T = &\frac{1}{1 + \frac{\gamma_{\mathrm{TM}} k_y^2}{\gamma_x (k_y^2 + k_p^2)} \tanh(\frac{\gamma_{\mathrm{TM}} d}{2}) - \frac{k k_p^2}{\gamma_x (k_y^2 + k_p^2)} \tan(\frac{kd}{2})} \\ &- \frac{1}{1 + \frac{\gamma_{\mathrm{TM}} k_y^2}{\gamma_x (k_y^2 + k_p^2)} \mathrm{ctanh}(\frac{\gamma_{\mathrm{TM}} d}{2}) + \frac{k k_p^2}{\gamma_x (k_y^2 + k_p^2)} \mathrm{ctan}(\frac{kd}{2})}. \end{aligned} \tag{1.8}$$

In the above ”tanh” and ”ctanh” represent the hyperbolic tangent and cotangent, respectively. It is important to note that the transmission coefficient T can be regarded as a transfer function: the image at the output plane is obtained by the superposition of the (TM-polarized) spatial harmonics of the source field distribution at the input plane multiplied by T. Thus, ideally, for perfect imaging, one should have $T = 1$, independent of k_y.

As mentioned in Sect. 1.2, the best strategy to achieve good imaging is to tune the thickness of the slab so that it verifies the Fabry-Perot condition, or equivalently $kd = n\pi$, where n is an integer. In this case (1.8) can be simplified: if $kd = (2n+1)\pi$ then

$$T = -\frac{1}{1 + \frac{\gamma_{\mathrm{TM}} k_y^2}{\gamma_x (k_y^2 + k_p^2)} \mathrm{ctanh}(\gamma_{\mathrm{TM}} d/2)}, \quad R = 1 + T, \tag{1.9}$$

whereas if $kd = 2n\pi$ then

$$T = \frac{1}{1 + \frac{\gamma_{\mathrm{TM}} k_y^2}{\gamma_x (k_y^2 + k_p^2)} \tanh(\gamma_{\mathrm{TM}} d/2)}, \quad R = 1 - T. \tag{1.10}$$

If the operating frequency is much smaller than the plasma frequency, i.e. $k \ll k_p$, then since $kd/\pi > 1$ one can assume that $\gamma_{\rm TM} d \gg 1$, and using the expressions (1.9) and (1.10) we obtain simple approximate formulae for the reflection and transmission coefficients:

$$T \approx \mp \frac{1}{1 + \frac{\gamma_{\rm TM} k_y^2}{\gamma_x (k_y^2 + k_p^2)}}, \quad R \approx 1 - \frac{1}{1 + \frac{\gamma_{\rm TM} k_y^2}{\gamma_x (k_y^2 + k_p^2)}}, \tag{1.11}$$

where the $\mp$ sign corresponds to the case in which the thickness of the slab is equal to an even or odd number of half-wavelengths, respectively.

It is clear that the imaging quality does not depend on the thickness of the structure. The transmission device can be made as thick as it may be required by an application. The only restriction is that the thickness has to be equal to an integer number of half-wavelengths. If the number of half-wavelengths is odd then the image at the back interface of the structure will appear out-of phase with respect to the source, whereas if the number of half-wavelengths is even then the image and the source will be in phase.

1.3.2 Parametric study of reflection and transmission properties

In order to characterize the typical behavior of wire medium lenses, we consider a structure with the same dimensions as that considered in the experimental work [21]. Thus, the lattice constant is taken equal to $a = 1$ cm and the radius of the wires is taken equal to $r = 1$ mm. The frequency of operation is 1GHz, which corresponds to $ka = 0.2$. The thickness of the lens is $d = 15$ cm, i.e. exactly half-wavelength at the frequency of operation ($kd = \pi$).

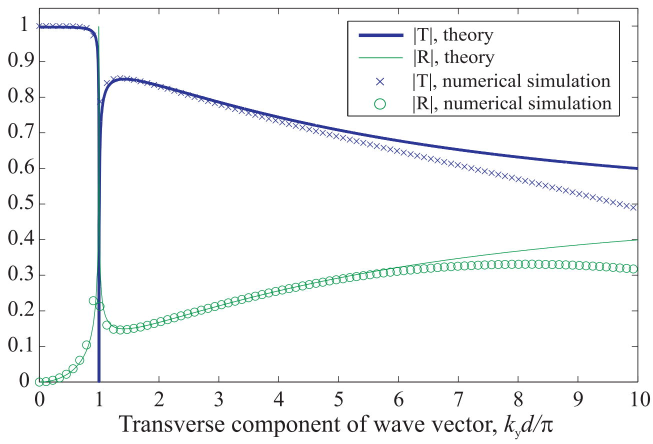

FIGURE 1.7 Reflection (R) and transmission (T) coefficients (absolute values) as a function of the transverse component of wave vector $k_y d/\pi$ for $kd/\pi = 1$. Solid lines: analytical expressions (1.7) and (1.8). Crosses and circles: points calculated using full wave numerical method.

The dependence of the reflection and transmission coefficients (absolute values) on the normalized transverse component of wave vector $k_y d/\pi$ is plotted in Fig. 1.7. One can see that the transmission coefficient has a very sharp dip at $k_y = k$, but for other values of k_y it has values close to unity. In Fig. 1.7 the "crosses" and "circles" represent the data calculated numerically using the periodic method of moments. As seen, the agreement between the analytical model and the full wave results is very satisfactory. The phase of the transmission coefficient (not shown here) is practically equal to π for whole range of k_y, except for a very narrow band centered close to k. The obtained dependence confirms that the slab indeed operates in the canalization regime and is capable of transporting sub-wavelength images with TM polarization.

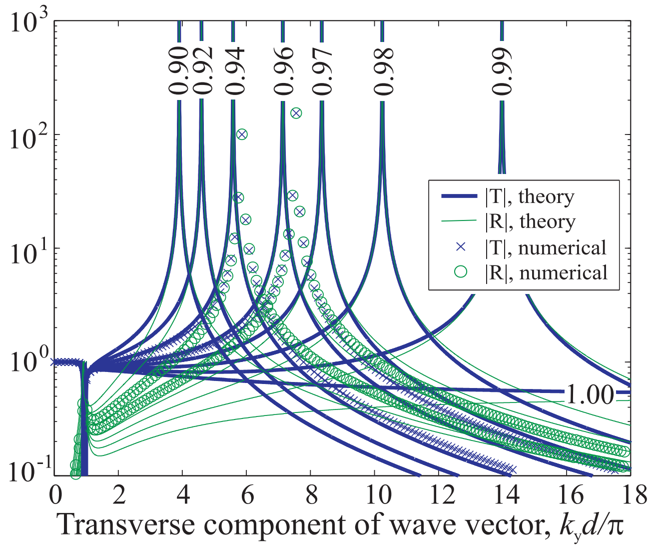

FIGURE 1.8 (Color online) Reflection (R) and transmission (T) coefficients (absolute values) as a function of the transverse component of wave vector $k_y d/\pi$ for $kd/\pi = 1 - 0.01n$, where n=0,1,2,3,4,6. The numbers in the figure correspond to the values of kd/π. The crosses and circles represent the results of the numerical modeling for $kd/\pi = 0.94$ and $kd/\pi = 0.96$.

The behavior of the transmission and reflection coefficients is sensitive to variations in the frequency of operation. If the frequency is slightly lower than the frequency of operation (corresponding to the Fabry-Perot condition) then a very interesting resonant phenomenon is observed. This is illustrated in Fig. 1.8, where the transmission coefficient is plotted for frequencies lower than the design frequency by $1, 2, 3, 4$ and 6%. One can observe a very strong enhancement of certain spatial harmonics. This property reveals the presence of guided modes propagating along the y direction of the slab. The resonant excitation of guided modes deteriorates the quality of sub-wavelength imaging since some of the spatial harmonics happen to be amplified by a factor of 10 or even more. Physically, this leads to appearance of 'ripples' both in the source and image planes of the wire medium lenses which were reported in [22, 20] and can be seen in Fig. 1.5.

For frequencies slightly larger than the frequency corresponding to the Fabry-Perot resonance, the reflection and transmission coefficients do not have a resonant behavior. This is shown in Fig. 1.9, where the reflection and transmission coefficients are plotted for frequencies larger than the design frequency by $1, 2$ and 4%. This means that the slab does not support guided modes in this frequency range. Further increase of the frequency (by 8 or 16%, for example, see Fig. 1.9) leads to the increase of the width of the narrow dip of the transmission characteristic at $k_y = k$, and to the appearance of resonances in the vicinity of this point. These resonances are also related with guided modes. The resonant behavior in the present case has a very narrow band character and does not significantly affect the

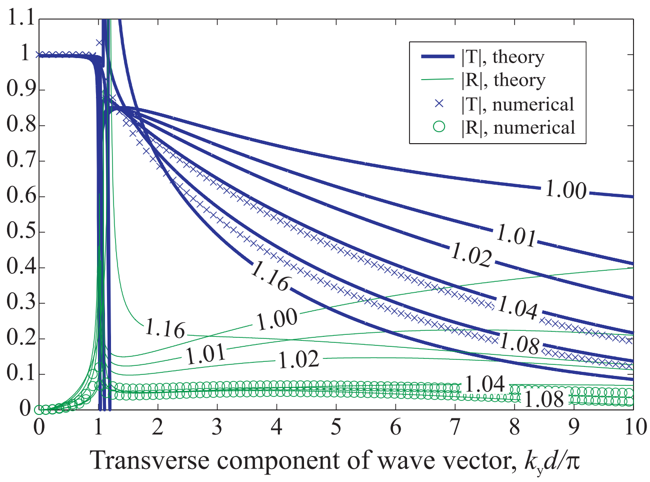

FIGURE 1.9 (Color online) Reflection (R) and transmission (T) coefficients (absolute values) as a function of the transverse component of wave vector $k_y d/\pi$ for $kd/\pi = 1 + 0.01n$, where n=0,1,2,4,8,16. The numbers in the figure correspond to the values of kd/π. The crosses and circles present the results of the numerical modeling for $kd/\pi = 1.04$ and $kd/\pi = 1.08$.

imaging properties of the device.

In Fig. 1.9 one can see a strong reduction of the reflection coefficient for $kd/\pi = 1.04$ and $kd/\pi = 1.08$. The reflection coefficient becomes less than 10% practically for the whole spatial spectrum. This fact has been confirmed both numerically [19] and experimentally [22], and means that for these frequencies there is little interference between the source and the signal reflected at the wire medium slab. However, the dependence of transmission coefficient on transverse wave vector becomes less flat when the frequency of operation is significantly greater than the Fabry-Perot resonance frequency. This leads to respective degradation of subwavelength imaging resolution provided by the wire medium slab [19, 22].

1.4 Magnifying and demagnifying lenses with super-resolution

Processing of subwavelength images, such as magnification or demagnification, can be performed by tapering the array of wires. Thus, by gradually increasing (decreasing) the spacing between wires from the front interface to the back interface, it is possible to magnify (demagnify) the subwavelength details of an image.

A numerical simulation of the tapered version of the 1-meter lens described in the section 1.2 was performed using a commercial electromagnetic simulator based on the Method of Moments (MoM) [26]. The geometry of the structure is presented in Fig. 1.10(a). The spacing between of wires at the front interface is 1 cm (as in Fig. 1.3) and it gradually increases up to 3 cm at the back interface. The front and back interfaces of the lens are spherical surfaces with 50 and 150 cm radii, respectively. The lens is excited by a planar center-fed wire antenna in the form of letter "M", which is placed in the close vicinity of the front interface. The frequency of operation (910 MHz) is chosen slightly higher than the Fabry-Perot resonance of the 6th order (900 MHz) in order to achieve the best quality of imaging [27].

This structure enables a three fold magnification of the source. This fact is clearly seen in Figs. 1.10(b) and (c) where the distributions of the normal (with respect to the interface)

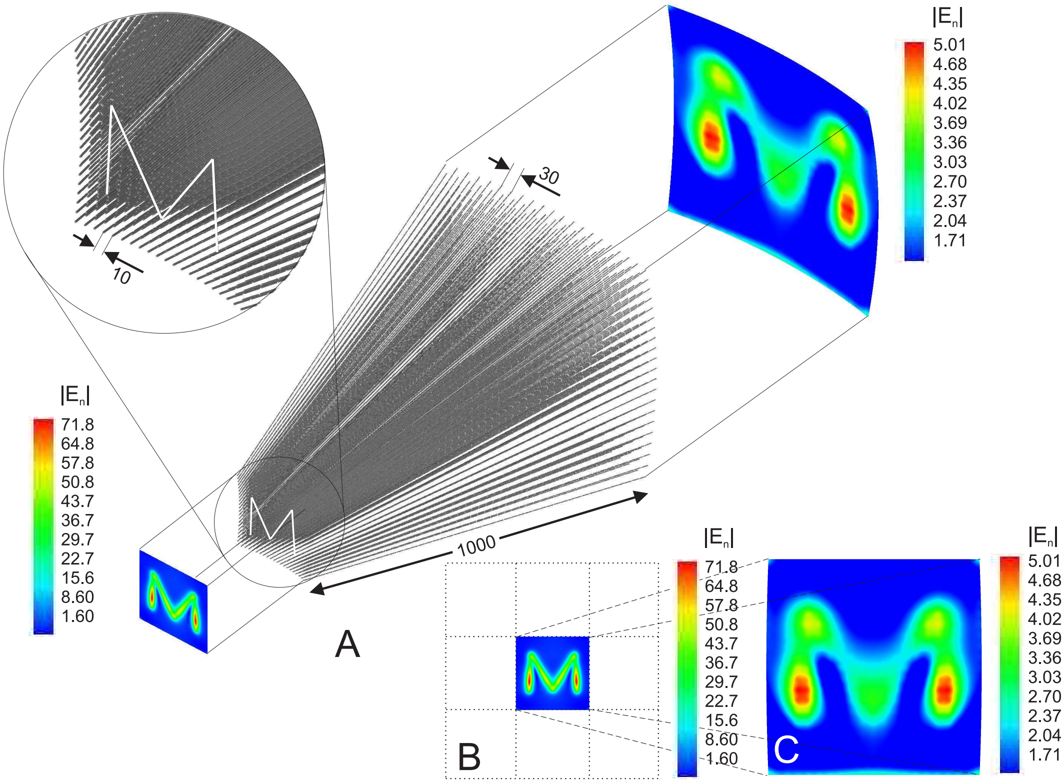

FIGURE 1.10 (a) Geometry of the magnifying wire medium lens excited by a planar near-field source shaped as the letter "M". The distance between the source and the center of the front interface is 13 mm. All the length dimensions in the figure are given in millimeters. Calculated distributions of the electric field normal component: (b) on a planar surface located (13+8)mm away from the lens input interface (the reference plane is displaced 8mm from the source) and (c) on a spherical surface displaced 15mm from the output interface. The frequency of operation is 910 MHz.

component of electric field at 8 mm distance from the source and 15 mm distance from the back interface are plotted. The distance in between the source and the image is about 3 wavelengths. In both figures a sharp near-field distribution in the form of the letter M is visible, but remarkably the image is magnified 3 times as compared to the original. A larger magnification is possible with a similar structure, but it requires the use of a thicker lens.

The proposed tapered lens [Fig. 1.10(a)] has spherical input and output interfaces, but some applications may require the use of planar interfaces. The difficulty of making a tapered lens with planar interfaces is that it inevitably requires the use of wires with different physical lengths. This may destroy the collective Fabry-Perot resonance and affect the performance of the lens. However, returning to the explanation that each wire of the lens operates as a separate subwavelength waveguide, one can conclude that the physical length of the wires does not really matter, provided its electrical length is invariant. Thus, provided the electrical length of the wires in a tapered lens with planar interfaces is constant, the lens may still operate as desired. One interesting possibility to make this phase compensation is to incorporate a properly shaped dielectric block inside of the lens.

Magnifying lenses are expected to find immediate application in near-field microscopy as near-field to far-field transformers [4, 5, 6, 7] since they may allow mapping field distributions with subwavelength details into images with details larger than the wavelength, which can be processed using conventional diffraction-limited imaging techniques. Also, tapered lenses may be used for demagnification of images if the source and image interfaces of the magnifying lens are interchanged. Demagnifying lenses may allow creating complex near-field distributions from enlarged copies created in the far-field. On this route, it may be possible to create extremely compact near-field spots which can be used for dense writing of information on various media, in the same manner as diffraction-limited laser spots are currently used for writing on DVD drives.

Tapered wire medium lenses, especially in the terahertz range, can be regarded as multipixel endoscopes capable of performing direct and inverse manipulations with the electromagnetic fields in the subwavelength spatial scale: capturing an electromagnetic field profile created by deeply subwavelength objects at the endoscope's tip and magnifying it for observation, or projecting a large mask at the endoscopes base onto a much smaller image at the tip [28].

In the microwave range the tapered wire medium endoscopes may be possibly applied for the improvement of magnetic resonance imaging (MRI) systems [29]. Such systems use small magnetic probes, whose dimensions determine the resolution of MRI. To ensure a reasonable efficiency the probes cannot be made much smaller than the wavelength. This obviously restricts the resolution of these systems. By placing the tapered wire medium lenses in between the object under test and the probe of the near-field scanner, it may be possible to further reduce the effective size of the probe keeping its efficiency at the same level, and improving in this way the resolution of MRI. Likewise, tapered wire medium endoscopes and lenses can be used to enhance the performance of other mechanical near-field microwave scanners suffering from similar problems. Instead of attempting to use small probes in order to improve resolution one can magnify the near-field distribution under test and detect the magnified distribution using a conventional probe. It is envisioned that the tapered lenses can be used in two ways: the tapered endoscope can be attached to the probe effectively reducing its size (in this case the scan is performed along the surface under test using the tip of the endoscope); or a large tapered lens can be attached to the whole sample under test and the magnified near-field distribution is scanned at the output interface of the lens.

1.5 Imaging at terahertz frequencies and beyond

The wire medium lenses described in the previous sections were designed to operate at the microwave frequency range. However, the structures may be easily scaled up to terahertz and even infrared frequencies provided the metal used to fabricate the rods maintains reasonable conductive properties. For example, in [30] it was reported that a wire medium lens made of silver (Ag) nanorods enables subwavelength resolution of $\lambda/10$ at 30 THz ($\lambda = 10\mu$m). Fig. 1.11 shows the results reported in [30] for imaging at 31THz.

The main difficulty with the extension of the wire medium lens concept to the terahertz and infrared regimes is that most metals do not exhibit strong conductive properties at these frequencies, but instead have a plasmonic response. This fact imposes some constraints on the implementation of the canalization regime at the infrared range using arrays of nanorods [30]. As demonstrated in [23], for real metals (with finite conductivity) the resolution of the "wire medium lens" cannot be further improved by reducing the spacing between the wires after the radius of the wires becomes smaller than the skin depth of the metal. In addition, for geometrical reasons the period of the array should be at least 2 times larger than the radius of rods. Since the resolution of a lens operated in the canalization regime is approximately two times the spacing between the wires [19], we can estimate that the ultimate physical limit of resolution of wire medium lenses is about 4 times the skin depth of the metal.

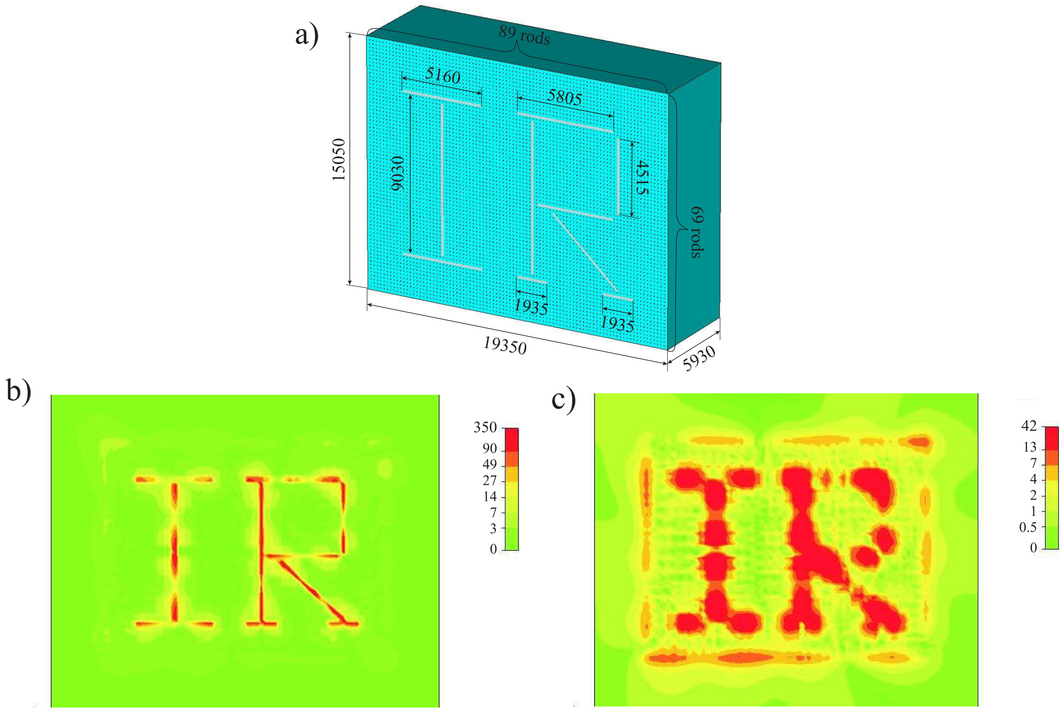

FIGURE 1.11 Numerical modeling of subwavelength imaging at 31THz ($\lambda = 10\mu$m) [30]. (a) Geometry of the lens: a square array with 215 nm period formed by silver nanorods with 21.5 nm radius embedded into a block of chalcogenide glass (relative permittivity $\varepsilon = 2.2$). All dimensions in the figure are given in nanometers. The lens is excited by a planar antenna shaped in the form of the letters 'IR', and located 107.5 nm apart from the front interface of the lens. Calculated distributions of the normal component of electric field: (b) at the front interface (source plane) and (c) at the back interface (image plane).

To give an idea of the possibilities, the limits of resolution yielded by rods of silver (Ag), gold (Au), aluminium (Al) and copper (Cu) at several frequencies are compiled in Table 1. It was assumed that the metals are described by a Drude model with the plasma and damping frequencies as in [31, 32]. It is seen that at microwave frequencies the ultimate limit

	100MHz	1GHz	10GHz	100GHz	1THz	10THz
Ag	$\lambda/116000$ ($26\mu m$)	$\lambda/37000$ ($8.2\mu m$)	$\lambda/11600$ ($2.6\mu m$)	$\lambda/3700$ ($0.8\mu m$)	$\lambda/1265$ ($237nm$)	$\lambda/320$ ($94nm$)
Au	$\lambda/95000$ ($32\mu m$)	$\lambda/30000$ ($10\mu m$)	$\lambda/9500$ ($3.2\mu m$)	$\lambda/3020$ ($1.0\mu m$)	$\lambda/1010$ ($297nm$)	$\lambda/300$ ($100nm$)
Al	$\lambda/90000$ ($33\mu m$)	$\lambda/28000$ ($11\mu m$)	$\lambda/9000$ ($3.3\mu m$)	$\lambda/2850$ ($1.1\mu m$)	$\lambda/923$ ($325nm$)	$\lambda/324$ ($93nm$)
Cu	$\lambda/75000$ ($41\mu m$)	$\lambda/23000$ ($13\mu m$)	$\lambda/7500$ ($4.1\mu m$)	$\lambda/2340$ ($1.3\mu m$)	$\lambda/776$ ($387nm$)	$\lambda/248$ ($121nm$)

TABLE 1.1 Ultimate limit of resolution of wire medium slabs for several metals and frequencies. The metals were characterized using the experimental data tabulated in [31].

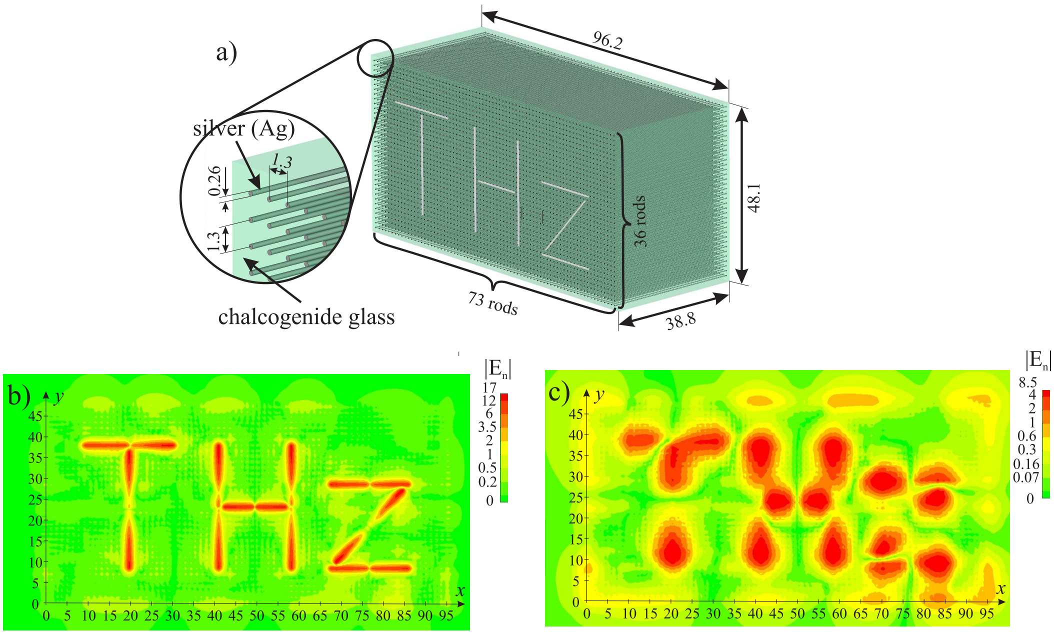

FIGURE 1.12 Numerical modeling of subwavelength imaging at 5THz ($\lambda = 60\mu$m) [23]. (a) Geometry of the lens: a square array with 1.3μm period formed by silver nanorods with 130 nm radius embedded into a block of chalcogenide glass (relative permittivity $\varepsilon = 2.2$). All dimensions in the figure are given in micrometers. The lens is excited by a planar antenna shapped in the form of the letters "THz", and located 650 nm apart from the front interface of the lens. Calculated distributions of the normal component of electric field: (b) at the front interface (source plane) and (c) at the back interface (image plane).

of resolution is several orders of magnitude larger than the classical diffraction limit, and that the best results are achieved with silver. Even at terahertz frequencies the resolution may be of the order of $\lambda/300$. In particular, one may conclude that at the terahertz range, arrays of parallel rods made of noble metals and their tapered versions may enable the same manipulations in the subwavelength spatial scale as their microwave counterparts [Figs. 1.3 and 1.10(a)]. The only difference is that the structures for the terahertz range are more difficult to fabricate.

To illustrate the potentials of wire medium lenses at terahertz frequencies, we consider the structure depicted in Fig. 1.12(a). The lens is formed by an array of silver nanorods supported by a block of chalcogenide glass, which has low losses at terahertz frequencies. The source antenna is shaped as the letters "THz" in order to emphasize the frequency of operation: 5 THz. The performance of the lens was simulated using the commercial electromagnetic solver [33]. The calculated near-field distributions at the front and back interfaces are presented in Figs. 1.12(b) and 1.12(c), respectively. The letters 'THz' are clearly visible in both distributions. The effect of realistic losses in silver at 5 THz [31, 32] was fully taken into account in the simulation. In this example the radius of the rods R was chosen so that $R = 4.8\delta$ (δ is the skin depth of silver), which enables very good imaging. The resolution in this example is $\lambda/23$ (2.6μm) and the image is formed at a distance 0.65λ (38.8μm) from the source.

Interestingly, high losses in the rods material may not affect the imaging performance provided the absolute value of permittivity is large enough. This happens because the field canalized through the lens is mainly concentrated in the host material in between the rods.

It is extruded from the rods because of their high permittivity. This means that extremely lossy materials, for example materials operated near absorption bands, may also be good candidates for the realization of wire media with extreme anisotropy.

Regarding fabrication issues, it has to be noted that the realization of wire medium lenses both in microwave and terahertz ranges does not need to be very precise. The lens performance is not sensitive to the exact locations of the rods in the matrix, variations of the radii of the rods, or to the precise shape of the rods cross-section. The only parameter that it is necessary to control is the length of the rods. It should be roughly the same for all rods, and the rods need to be continuous. Broken rods or rods with conductivity defects may significantly affect the imaging quality.

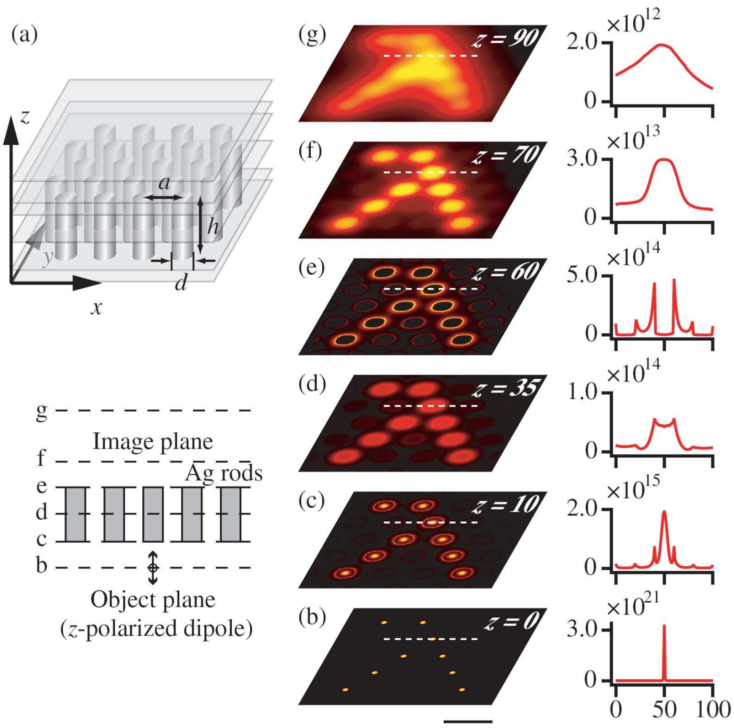

FIGURE 1.13 Subwavelength plasmonic image transfer of a character pattern λ with a metallic nanorod array device [34]. (a) The structural model of the device, which is constructed by hexagonally arranged silver nanorods of 20 nm diameter, 50 nm height, and with 40 nm pitch, respectively. (b)(g) Field propagation process in the image transfer obtained at each longitudinal position by the FDTD simulation. The character pattern is composed of an array of z-polarized dipoles. Left side images show the cross-sectional intensity distributions in the x-y plane. The plots on the right side show the cross-sectional line profiles of dashed lines in the left images. The object plane and imaging plane are defined as $z = 0$ and $z = 70$nm. The operation wavelength is 488 nm. The size of the scale bar is 50 nm.

In the visible frequency range it may also be possible to achieve subwavelength imaging using metallic nanorods [34], see Fig. 1.13. This possibility is based on the excitation of surface plasmon polaritons in the metallic rods. However, this regime is highly sensitive to losses, and may introduce important phase and amplitude distortions in the image due to the harmful interaction among surface plasmons traveling along adjacent rods. In particular, this may result in the impossibility of resolving certain source field distributions at the image plane.

References

[1] J. Pendry, "Negative refraction index makes perfect lens," *Phys. Rev. Lett.*, vol. 85, pp. 3966–3969, 2000.

[2] N. Fang, H. Lee, C. Sun, and X. Zhang, "Subdiffraction-limited optical imaging with a silver superlens," *Science*, vol. 308, pp. 534–537, 2005.

[3] E. E. Narimanov and V. M. Shalaev, "Beyond diffraction," *Nature*, vol. 447, pp. 266–267, 2007.

[4] A. Salandrino and N. Engheta, "Far-field subdiffraction optical microscopy using metamaterial crystals: Theory and simulations," *Phys. Rev. B*, vol. 74, p. 075103, 2006.

[5] Z. Jacob, L. V. Alekseyev, and E. Narimanov, "Optical hyperlens: Far-field imaging beyond the diffraction limit," *Optics Express*, vol. 14, pp. 8247–8256, 2006.

[6] I. I. Smolyaninov, Y.-J. Hung, and C. C. Davis, "Magnifying superlens in the visible frequency range," *Science*, vol. 315, pp. 1699–1701, 2007.

[7] Z. Liu, H. Lee, Y. Xiong, C. Sun, and X. Zhang, "Far-field optical hyperlens magnifying sub-diffraction-limited objects," *Science*, vol. 315, p. 1686, 2007.

[8] V. Westphal and S. W. Hell, "Nanoscale resolution in the focal plane of an optical microscope," *Phys. Rev. Lett.*, vol. 94, p. 143903, 2005.

[9] P. Belov, R. Marques, S. Maslovski, I. Nefedov, M. Silverinha, C. Simovski, and S. Tretyakov, "Strong spatial dispersion in wire media in the very large wavelength limit," *Phys. Rev. B*, vol. 67, p. 113103, 2003.

[10] M. Silveirinha, "Nonlocal homogenization model for a periodic array of epsilon-negative rods," *Phys. Rev. E*, vol. 73, p. 046612, 2006.

[11] P. Belov and Y. Hao, "Subwavelength imaging at optical frequencies using a transmission device formed by a periodic layered metal-dielectric structure operating in the canalization regime," *Phys. Rev. B*, vol. 73, p. 113110, 2006.

[12] P. A. Belov, C. R. Simovski, and P. Ikonen, "Canalization of sub-wavelength images by electromagnetic crystals," *Phys. Rev. B.*, vol. 71, p. 193105, 2005.

[13] V. A. Podolskiy and E. E. Narimanov, "Near-sighted superlens," *Opt. Lett.*, vol. 30, pp. 75–77, 2005.

[14] T. Yen, W. Padilla, N. Fang, D. Vier, D. Smith, J. Pendry, D. Basov, and Z. Zhang, "Tetrahertz magnetic response from artificial materials," *Science*, vol. 303, pp. 1494–1496, 2004.

[15] S. Linden, C. Enkrich, M. Wegener, J. Zhou, T. Kochny, and C. Soukoulis, "Magnetic response of metamaterials at 100 tetrahertz," *Science*, vol. 306, pp. 1351–1353, 2004.

[16] S. Zhang, W. Fan, N. C. Panoiu, K. J. Malloy, R. M. Osgood, and S. R. J. Brueck, "Experimental demonstration of near-infrared negative-index metamaterials," *Phys. Rev. Lett.*, vol. 97, p. 137404, 2005.

[17] V. M. Shalaev, "Optical negative-index metamaterials," *Nature Photonics*, vol. 1, pp. 41–48, 2007.

[18] P. Ikonen, P. A. Belov, C. R. Simovski, and S. I. Maslovski, "Experimental demonstration of subwavelength field channeling at microwave frequencies using a capacitively loaded wire medium," *Phys. Rev. B*, vol. 73, p. 073102, 2006.

[19] P. A. Belov and M. G. Silveirinha, “Resolution of sub-wavelength lenses formed by a wire medium,” *Phys. Rev. E*, vol. 73, p. 056607, 2006.

[20] P. A. Belov, Y. Zhao, S. Tse, P. Ikonen, M. G. Silveirinha, C. R. Simovski, S. Tretyakov, Y. Hao, and C. Parini, “Transmission of images with subwavelength resolution to distances of several wavelengths in the microwave range,” *Phys. Rev. B*, vol. 77, p. 193108, 2008.

[21] P. A. Belov, Y. Hao, and S. Sudhakaran, “Subwavelength microwave imaging using an array of parallel conducting wires as a lens,” *Phys. Rev. B*, vol. 73, p. 033108, 2006.

[22] P. Belov, Y. Zhao, S. Sudhakaran, A. Alomainy, and Y. Hao, “Experimental study of the sub-wavelength imaging by a wire medium slab,” *Appl. Phys. Lett.*, vol. 89, p. 262109, 2006.

[23] M. G. Silveirinha, P. A. Belov, and C. R. Simovski, “Ultimate limit of resolution of subwavelength imaging devices formed by metallic rods,” *Opt. Lett.*, vol. ??, p. ????, 2008.

[24] P. Belov, S. Tretyakov, and A. Viitanen, “Dispersion and reflection properties of artificial media formed by regular lattices of ideally conducting wires,” *J. Electromagn. Waves Applic.*, vol. 16, p. 1153, 2002.

[25] M. Silveirinha, “Additional boundary condition for the wire medium,” *IEEE Trans. Antennas. Propagat.*, vol. 54, pp. 1766–1780, 2006.

[26] FEKO Suite 5.2, EM SOftware & Systems - SA (Pty) Ltd, http://www.feko.info.

[27] P. Ikonen, C. Simovski, S. Tretyakov, P. Belov, and Y. Hao, “Magnification of subwavelength field distributions at microwave frequencies using a wire medium slab operating in the canalization regime,” *Appl. Phys. Lett.*, vol. 91, p. 104102, 2007.

[28] G. Shvets, S. Trendafilov, J. B. Pendry, and A. Sarychev, “Guiding, focusing, and sensing on the subwavelength scale using metallic wire arrays,” *Phys. Rev. Lett.*, vol. 99, p. 053903, 2007.

[29] X. Radu, X. Dardenne, and C. Craeye, “Experimental results and discussion of imaging with a wire medium for mri imaging applications,” in *Proc. of IEEE Antennas and Propagation Society International Symposium*, 2007, pp. 5499–5502.

[30] M. Silveirinha, P. Belov, and C. Simovski, “Sub-wavelength imaging at infrared frequencies using an array of metallic nanorods,” *Phys. Rev. B*, vol. 75, p. 035108, 2007.

[31] M. A. Ordal, R. J. Bell, R. W. Alexander, L. L. Long, and M. R. Querry, “Optical properties of fourteen metals in the infrared and far infrared: Al, co, cu, au, fe, pb, mo, ni, pd, pt, ag, ti, v, and w.” *Applied Optics*, vol. 24, pp. 4493–4499, 1985.

[32] I. El-Kady, M. M. Sigalas, R. Biswas, K. M. Ho, and C. M. Soukoulis, “Metallic photonic crystals at optical wavelengths,” *Phys. Rev B*, vol. 62, pp. 15 299–15 302, 2000.

[33] CST Microwave Studio 2006, CST GmbH, http://www.cst.com.

[34] A. Ono, J. Kato, and S. Kawata, “Subwavelength optical imaging through a metallic nanorod array,” *Phys. Rev. Lett.*, vol. 95, p. 267407, 2005.